Effect of Compressive Force on the Performance of a Proton Exchange Membrane Fuel Cell (PEMFC)

T. Ous and C. Arcoumanis

Energy and the Environment Research Centre

School of Engineering & Mathematical Sciences, The City University London

Abstract

The effect of the compressive force on the performance of a proton exchange membrane fuel cell (PEMFC) has been examined experimentally. The performance has been evaluated on the three polarization regions of the cell: activation, ohmic and mass transport. Measurements of the cell voltage and current density as a function of pressure were performed under constant load and various inlet air humidity conditions. The pressure distribution on the surface of the gas diffusion layer (GDL) was measured using a pressure detection film and the results show that increasing the pressure improves the performance of the cell. However, very high pressure can cause a dramatic decline in performance. The mass transport region proved to be the most susceptible to compression relative to the other two polarization regions. Furthermore, the performance was slightly more affected by compression under dry air than under humid air conditions.

Keywords: PEMFC; Compression; Performance; Torque; Gas diffusion layer (GDL).

1. Introduction

The compressive force applied to a single or stack fuel cell design influences a number of mechanical, electrical and probably chemical properties of fuel cells. Some of these changes are advantageous in terms of performance, whereas others can be detrimental. Not enough clamping pressure between the fuel cell plates can result in leakage of both reactants from the active flow channels. The interfacial contact resistance between the plates can also be very high. Too much pressure, on the other hand, can cause deformation to some of these plates minimising the electrical conducting area within the cell. It may even damage some brittle components of the cell such as the Gas Diffusion Layer (GDL) or the thin reactant-flow plates. In all cases, changes in fuel cell performance can take place. Thus an investigation to identify the optimum assembly pressure for an enhanced fuel cell is fundamental and necessary.

The impact of compression on the interfacial contact resistance between some of the fuel cell plates has been investigated previously [1 – 3]. In particular, the through-plane resistance of a Toray carbon paper (GDL) was characterised under various applied torque loads [1]. The approach was to apply a defined compaction force across the plate-GDL-plate assembly, pass a D.C. current through and measure the plate-to-plate voltage drop. The results have shown an exponential reduction of the total resistance, bulk and contact resistance, with increasing compression. A similar technique was used in [2] to measure the contact resistance of GDL and various reactant-flow plate materials. The contact resistance was again found to reduce exponentially with compression. In [3], the contact resistance was estimated during the operation of a fuel cell by measuring the voltage between the current collector plate and the GDL under two different compaction pressures. The measured voltage was plotted against the cell current density

yielding a straight line whose slope was interpreted as contact resistance. The results indicate that higher compaction pressures induce lower contact resistance. The reduction of contact resistance caused by compression was found to be even more significant than trends observed in GDL's contact resistance for various flow-plate alloys such as graphite or stainless steel [4]. In [5] the pressure distribution on the surface of the GDL was simulated by a Finite Element Analysis (FEA) model which was validated using a sensitive pressure film inserted between the reactant-flow plate and the membrane electrode assembly (MEA). It should be noted that the method of applying pressure across the fuel cell end-plates affects the pressure distribution within the cell. As the assembly of most fuel cells is based on the traditional point-load design, the local pressure around the clamping areas is expected to be higher than in other locations. This, however, may not show the true effect of compression on the performance of fuel cells. The compaction force across the cell should in principle be applied in such a way that pressure is equally distributed along the entire surface of the cell. The hydro-pressure technique used in [6] has produced a better pressure distribution than the traditional design; the fuel cell polarisation curves showed that cells under uniform pressure have better performance than the traditional point-load design, and that compression enhances the performance of the cell linearly. The experimental work in [7] has also investigated the effect of pressure directly onto the fuel cell polarisation curve. Three different GDL types were examined and the results showed that each of them exhibited different optimal assembly pressure for performance enhancement of the cell.

Here the effect of uniform-surface compression on the performance of fuel cells is investigated by inserting a pressure detection film between the GDL and the reactant-flow plates to measure the pressure distribution on the GDL surface. The change in performance as a function of pressure was analysed in the three polarisation regions under different air humidity conditions. Furthermore, measurements of the cell voltage and current density as a function of pressure were performed separately under constant resistance load.

2. Theory
The use of compaction pressure during the assembly of fuel cells plays a crucial role particularly at the interface between the GDL and the reactant-flow plates. It reduces the interfacial contact resistance between those two parts as well as it serves as sealant to ensure proper delivery of reactants to the active flow channels. However, the increase in pressure must be controlled accurately since it may cause damage to some components of the cell. If the reactant-flow plate breaks, the reactants can escape from the reaction channels to the outer side of the cell; alternatively they can cross from channel to channel making less use of the active area of the catalyst. In addition, the bulk resistance of the reactant-flow plate becomes higher and the same applies to the GDL. Any hole or broken strip on the surface of the GDL allows the reactants to cross more easily from the anode to the cathode, or visa versa, increasing the amount of fuel crossover. The reactants can also flow directly from the channels into the catalyst layer without being uniformly distributed on the surface of the catalyst. Finally, the conducting area between the GDL and the catalysts will be reduced.

2.1 Effect on fuel cell resistance
The fuel cell resistance can be calculated by the summation of the bulk and interfacial contact resistances of all the adjacent plates within the electrical network of the cell, as illustrated in

Figure 1. This includes the current collector plates, reactant-flow plates, gas diffusion carbon layers and the Membrane Electrode Assembly (MEA) sandwiched in the middle.

Figure 1 Equivalent circuit of the total resistance for one side electrode fuel cell

The fuel cell resistance R_{FC} can be calculated as

$$\boxed{}$$

$$(1)$$

$$\boxed{}$$

$$(2)$$

$$\boxed{}$$

$$(3)$$

where R_{Bulk} is the bulk resistance of the fuel cell plates, $R_{Contact}$ is contact resistance between the plates, R_M is the ionic resistance of the membrane, R_{CA} is the resistance of the catalyst, R_{GDL} is the resistance of the gas diffusion layer, R_{RP} is the resistance of the reactant-flow plates, R_{CC} is the resistance of the current collector plates, $R_{CC/RP}$ is the contact resistance of current collector/reactant-flow plate interface, $R_{RP/GDL}$ is the contact resistance of reactant-flow plate/gas diffusion layer interface, $R_{GDL/CA}$ is the contact resistance of gas diffusion layer/catalyst interface, and finally $R_{CA/M}$ is contact resistance of catalyst/membrane interface.

The membrane resistance R_M has the highest value among the other terms of Equations (2) and (3). It is a strong function of the water content and depends on the chemical properties of the Nafion used. The contact resistance values indicated in Equation (3) are very difficult to be measured since it is experimentally difficult to insert a measuring probe precisely at the exact location within the micro-scale interface region. A more feasible way to obtain these values is to measure the total resistance of the electrical chain, bulk and contact resistance, then subtract it from the bulk resistivity of each layer. Measuring the resistance of a 7-layer membrane type (GDL is hot pressed with the MEA on each side) enables to quantify the summation of $R_M, R_{EL,} R_{GDL,} R_{GDL/CA}$,

and $R_{CA/M}$ of Equations (2) and (3). The resistance of the reactant-flow plate R_{RP} and the current collector plate R_{CC} can be simply estimated by applying the body resistance equation below, i.e.

$$\boxed{}$$

(4)

where R is the plate resistance, $?$ is the resistivity of the material, d is the travelling length of the electron or the plate thickness, and A is its cross-sectional area.

Due to the presence of water as a result of the electrochemical reaction of the cell, the surface of a metal reactant-flow plate becomes corroded after a certain operating time. A passive film is then formed at the GDL/reactant-flow plate interface which increases the contact resistance significantly [3]. The thickness of the film is a function of the cell operating time and is strongly dependent on the pressure applied across the plates. By taking into account the film resistance, the effective resistance of fuel cell $R_{FC(eff)}$ becomes

$$\boxed{}$$

(5)

where R_{film} is the resistance of the passive film and t is the operating time.

The values of R_{film} and $R_{RP/GDL}$ are expected to be the most affected by compression. If a torque (()) is applied across the cell, Equation (5) becomes

$$\boxed{}$$

(6)

In order to express quantitatively the effect of compression and associate it with the fuel cell voltage, the empirical equation of the cell voltage V must be used

$$\boxed{}$$

(7)

where E_{rev} is the reversible potential at the exchange current density, B is the Tafel slope constant, i is the current density, i_o is the exchange current density, and i_n is the internal and fuel crossover equivalent current density.

Substitution of (6) into (7) gives

$$\boxed{}$$

(8)

2.1 Effect on mass transport

The porosity of the gas diffusion layer (GDL) facilitates the access of reactants into the fuel cell electrodes. By compressing the GDL, its thickness and effective porosity decreases, thus limiting the amount of reactants entering the electro-catalyst sites. The change in porosity can be estimated from the change in the layer thickness [1] as

$$\boxed{}$$

(9)

where $D_{bulk,o}$ is the bulk density of the diffusion media when uncompressed, $D_{real,}$ is the real density of the solid phase, and d_o, d are the thickness of the compressed and uncompressed layers, respectively.

The fuel cell current I is related to the mass flowrate of both reactants, oxygen and hydrogen, as

$$\boxed{}$$

(10)

$$\boxed{}$$

(11)

$$\boxed{}$$

where is the Faraday constant, and are the oxygen and hydrogen flowrates, respectively.

If the porosity of the diffusion layer reduces, the current calculations in Equations (10) and (11) become

$$\boxed{}$$

(12)

$$\boxed{}$$

The pressure acting on the diffusion layer at the land interface of the reactant-flow plates reduces the porosity especially under the land areas. This, however, minimises the possibility for the reactants to cross from one channel to another, the so-called channel-channel crossover. The pressure can also cause a slight deflection of the membrane into the channels; the amount of deflection varies depending on the layer's stiffness, compression load, temperature, and hydration of the membrane. This can result in changes to the flow and consumption of reactants in the channels. The effect is probably negligible once the channel is flooded with liquid water, but it can be avoided by making the channel length/width ratio less than 3 [8].

2.2 Effect on membrane electrode assembly (MEA)

During the operation of fuel cell, hydrogen protons migrate through the polymer membrane over a fixed distance governed by its actual thickness (~50 - 175(m). By applying more compression across the membrane, its thickness reduces. The distance which protons have to travel across the electrodes thus becomes shorter leading to a faster electrochemical reaction by the cell. This change has a minimal impact on the performance of fuel cells [9]. Compression also improves the efficiency of the catalyst utilisation. The surface area (SA) of the catalyst is a measure of the number of surface atoms to bulk atoms and is expressed as [10]

(14)

where D and r are the density and radius of atoms, respectively.

When compression is applied, the distribution of the catalyst atoms (e.g. Pt atoms) changes in such a way that more atoms tend to be at the surface, thus increasing the active surface area of the catalyst. In addition, compression may reduce the interatomic distances between the Pt atoms providing more favourable sites for the dissociative adsorption of oxygen during the reaction of the cell [4].

3. Experiment

3.1 Experimental set-up

The experimental set-up is illustrated in Figure 2. The hydrogen and air flow were regulated by the mass flow controllers CT Platon and JonCons, respectively which the reactant air was humidified (Norgren LO7-200-MPQG) before entering the cell. The pressure of the inlet reactant gases was measured using Stiko pressure indicators. The humidity and temperature of the inlet

and outlet air were measured using built-in k-type sensors (Honeywell HIH-3610 and HEL-700 series). Data was transferred into a PC via the data acquisition system (National Instruments PCI-6225), and the results were collected using compatible Labview 7 software. The compression unit, shown in Fig. 3, allows a gradual increase of the pressure across the end-plates of the cell. The screw located at the back of the unit is controlled by a torque wrench device and it pushes a flat metal plate in the horizontal direction towards the cell. The screw is. The fuel cell uses a Johnson Matthey membrane-electrode-assembly (MEA No. W11067-06, Pt loading $3.5mg/m^3$, active area $25cm^2$) sandwiched between two Toray carbon papers (TGP-H-060). The flow channels of both the anode and cathode were machined in serpentine shapes with a channel width of 1.5mm, a depth of 1.5mm, and a length of 655mm. The total number of channels in each plate was 13 and were equally spaced by lands, also called the ribs, of 1.5mm width. The fuel cell voltage and current density were measured using a multimeter (Black Star 3225) which the external load used in the measurements was a series of electric resistors, manually placed across the fuel cell unit.

Figure 2 Schematic diagram of the experimental set-up

Figure 3 Design of compression unit

3.2 Pressure distribution measurements

By applying the screw thread mechanics theory, it is possible to estimate from the torque of the compression unit the pressure distribution on the surface of the gas diffusion layer. A pressure detection film (Pressurex) was inserted between the diffusion layer and the reactant-flow plate to measure the pressure distribution on the surface. Sample pieces detecting pressures between $0.19MNm^{-2}$ and $9.65MNm^2$ were cut at similar dimensions to the cell plates. After each test, the film was removed and colour intensity processing was conducted to quantify the pressure distribution. Figure 4 shows the colour intensity for a torque of 22Nm. The white strips represent the channels in the reactant-flow plates whereas the red areas represent the graphite solid phase. Test repeated within the torque range 8 – 22Nm provided the required calibration with pressure (see Table 1).

3.3 Operating conditions

The fuel cell was operating at ambient conditions and was kept in operation to reach steady-state before measurements of voltage and current density were taken. The air enters the cell with a humidity of 100% RH whereas the inlet hydrogen was kept dry; the airflow was set to a stoichiometry of 2.3 (at current density of $128mA/cm^2$).

Figure 4 Pressure distribution on the surface of the GDL at 22Nm torque load

Table 1. Calibration between the pressure on the surface of the GDL and the applied torque

4. Results and discussion

4.1 Effect on fuel cell polarization curve

Figure 5 shows the fuel cell polarization curves under various pressure loads in the range 8-22Nm. It can be seen from the figure that compressing the cell within 8 – 12Nm improves its performance whereas higher compression (>12Nm) causes a dramatic decline in performance. The observed changes tend to be small at low current densities (activation region) but become significant at high current densities (ohmic and mass transport regions). As torque increases from 0 to 12Nm, the maximum change in the power density of the cell, which occurs in the mass transport region, increases from 47mW/cm² to 65mW/cm²; this gives a total amount of power

gained for the 25cm² cell size of 457mW. The power enhancement is maximum between 0 and 8Nm load, and more consistent between 8 – 12Nm torque range. At a current density of 60mA/cm², the cell voltage for 0Nm was 640mV. This value was increased to 710mV as the torque rose to 8Nm; from 8 to 12Nm, the value increased by only 14mV for each 2Nm increment of torque, giving an enhancement rate of 7mV for each 1Nm of applied torque.

Figure 5 Fuel cell polarization curves under various applied torque loads

4.1.1 Activation region

It was shown in Figure 5 that the change of performance in the activation region was smaller compared to the ohmic and mass transport regions. This implies that compression has generally more influence on the internal resistance and the water management of the cell than on the structure of the cell catalyst. The effect of compression on the speed of the electrochemical reaction of the catalyst can be identified from the activation behaviour of the cell, or Tafel plot in Figure 6, under torque loads of 0, 8, 10, and 12Nm. These results indicate that higher compression increases the reaction rate of the catalysts which can be deduced from the value of the exchange current density i_o. The exchange current density, i_o defined as the current density at which the overvoltage begins to move from zero. It can be obtained by plotting a tangent to the curves of

Figure 6 at a point (e.g. 2) where the curves become more stable in the log current density axis [11]; the interception of this line with the horizontal axis (log of the current density) gives its actual value. High values of i_o, mean higher catalyst reaction rate. The value of i_o can be calculated using the Tafel equation below given as

$$$$

(15)

where V is the cell overvoltage, i is the current density, and B is the Tafel slope constant obtained from [12]

The tangents plotted in Figure 6 at log current density value of 2 for 0Nm and 12Nm torque loads show that the exchange current density i_o slightly increases from 0-12Nm. The amount of current gained by compression means that the reaction of the electro-catalyst becomes faster, and that the active area of the electrodes has increased by a similar amount.

Fig. 6 Tafel Plots for different applied torque loads

Fig. 6 Tafel plots for different applied torque loads

4.1.2 Ohmic region

The change in the internal resistance of the fuel cell can be obtained directly from the ohmic region of the polarization curve. By measuring the change in the current density of the cell at fixed cell voltage values, the change in the area specific resistance of the cell can be calculated. Figure 7 shows the variations in the ohmic region for 0–12Nm torque range loads. At 0.7V cell potential, the change in the current density $?i$ between 0, 8, 10 and 12Nm torques is estimated to be 13mA/cm^2, 9mA/cm^2, and 9mA/cm^2, respectively. Using Ohm's law, the change in the area specific resistance for various loads can be calculated. The results show that the area specific resistance of the cell at 0Nm has decreased by almost 65% from its initial value when a torque of 12Nm was applied. This is quite a significant amount of power especially for a relatively low

power fuel cell.

Figure 7 Effect of compressive force in the ohmic region of a polarization curve

4.1.3 Mass transport region

The change in the mass transport region of a polarization curve is considered to be the most critical for the performance of fuel cells. Figure 8 shows the effect of different torque loads on the mass transport region of the cell. It can be seen that compressing the cell up to a value of 12Nm improves its performance. The current density, for a 0.01(load resistance, was extended from 104mA.cm^{-2} to 128mA.cm^{-2} when the torque increased from 0Nm to 12Nm. For each increment of 1Nm, within the 8 – 12Nm range, the cell gains an average amount of current density of 1mA.cm^{-2}. However, as the torque increases further to 14Nm, the maximum current density of the cell starts to drop (~ 4mA.cm^2). The limiting current density for torque loads of 14, 16, 18, 20, and 22Nm is estimated to be 116, 104, 76, and 38mA.cm^{-2}, respectively. This massive drop in the cell current implies that high compression, together with the associated excessive water generated by the cell, reduces tremendously the porosity of the gas diffusion layer, thus limiting the amount of reactants entering the electro-catalyst layer of the membrane and causing degradation. From the limiting current density values, an estimation of the change in the GDL porosity can be made. For instance, the limiting current at 16Nm has fallen by almost three times as the torque reaches 22Nm; the porosity of the GDL is thus expected to exhibit a similar decrease.

Figure 8 Effect of compressive force in the mass transport region of a polarization curve

4.2 Effect on fuel cell performance at constant loads

Figure 9 shows the change in fuel cell voltage within the 0Nm-12Nm torque range under fixed external loads (0.01?, 0.33? and 10?). These resistance values have been selected as they were able to measure, according to the results of Figure 5, the performance of the cell in the three polarization regions. The resistance value of 0.01? refers to the mass transport, 0.33? to the ohmic, and 10? to the activation region. As torque increases from 0–12Nm, also shown in Table 2, the change in the ohmic region was ~76mV. This change was larger than the activation (4mV) and the mass transport (58mV) regions. Figure 10 shows the variations in the current density for the same loads used in Figure 9. The current density in the activation domain was almost constant whereas the highest change was measured in the mass transport domain. In particular, the change in the current density within the 0Nm-12Nm range was estimated to be 0.6%, 13% and 23% for the activation, ohmic and mass transport regions, respectively.

Figure 9 Variation in cell voltage for different electronic loads

Figure 10 Variation in cell current density for different electronic loads

Figures 11 and 12 show the effect on fuel cell voltage and current density for the entire load range (0 – 22 Nm) examined. These graphs can be divided into three main parts. In the first region, from 0-14Nm, both voltage and current density values increase linearly by an amount of 13% for each 1Nm of applied torque. As the torque exceeds 14Nm, the slope of that change becomes less steep making the values almost constant. After a torque of 20Nm, a dramatic decrease in the performance occurs. This decline should be associated with the decrease in porosity of the GDL, as explained earlier. Table 2 lists the changes in the various quantities for the three polarization regions.

Figure 11 Variation of the cell voltage in the ohmic region (0.33?) as a function of compressive torque loads (0 – 22Nm)

Figure 12 Variation of the cell current density in the ohmic region (0.33?) as a function of compressive torque loads (0 – 22Nm)

Table 2 Variation of fuel cell voltage and current density in the three polarization regions

4.3 Effect on fuel cell performance at different air humidity

Figures 13 and 14 show the change in cell voltage and current at 0.33? resistance load for two air humidity conditions (50%RH and 100% RH). The measurements indicate that under more dried air conditions (50% RH) the performance of the fuel cell was slightly more affected by compression than when air humidity was higher. The change in the cell voltage and current values within the torque range of 8–18Nm for 50% was 67mV and 121mA, and for 100% RH was 58mV and 112mA, respectively.

Figure 13 Effect of compressive force on fuel cell voltage for different air humidity

The fuel cell current was estimated to decrease by an amount of 24mA, with respect to compression, as air humidity increases from 50% to 100% RH. A reasonable explanation for this result is related to the water content in the gas diffusion layer (GDL) of the cell. As argued previously, the contact and bulk resistance of the GDL are reduced by compression; the magnitude of reduction is less when the internal pores of this layer are empty of water under dry conditions than when they are filled with water.

Figure 14 Effect of compressive force on fuel cell current for different air humidity

5. Conclusions

A compressive force was applied across a PEM fuel cell in order to study possible effects on its performance. At each pressure load, measurements of cell voltage and current density were performed. The results show that increasing the torque up to a value of 12Nm improved the performance of the cell. The improvement of the cell voltage in the ohmic region was found to be the highest when compared with the activation and mass transport t regions whereas for the cell current density the mass transport region exhibited the highest change. However, the fuel cell performance declined dramatically, except for the activation region, when excessive pressure ((22Nm) was applied. In the ohmic region, the voltage and current density values of the cell decreased by 31% relative to their original values. The high compressive force probably caused a deflection to some plates in the cell design which increased the cell internal resistance. In the mass transport region, the performance of the cell was reduced significantly. The voltage and current density values dropped by 54% and 56%, respectively. This drop was the result of a large decrease in the porosity of the gas diffusion layer which limited the amount of reactants entering the electro-catalyst layer of the membrane. Under constant resistance load, the fuel cell voltage and current responded in a similar manner to compression by improving quite linearly with compression up to a torque load of 18Nm. They then remained constant between 18 – 20Nm, but declined dramatically at higher torques ((22Nm). Finally, the effect of compression on the performance of the cell was found to be more significant for dried rather than for humid air conditions.

Acknowledgement

Nomenclature

A	cross sectional area
B	Tafel constant
d	uncompressed thickness
do	compressed thickness
Dbulk,o	bulk density
Dreal	real density
V	cell voltage
E	reversible open circuit voltage
F	Faraday constant
i	Current
in	internal current
io	exchange current density
I	cell current
n	cell number
P	power
r	atom radius
R	resistance
RCA	catalyst resistance
RCC	current collector resistance
Rfilm	film resistance
RFC	fuel cell resistance
RFC(eff)	effective fuel cell resistance
RGDL	gas diffusion layer resistance

```
|RM         |membrane resistance                     |
|RRP        |reactant plate resistance               |
|RCA/M      |catalyst/membrane contact resistance    |
|RCC/RP     |current collector/reactant plate contact|
|           |resistance                              |
|RGDL/CA    |gas diffusion layer/catalyst contact    |
|           |resistance                              |
|RRP/GDL    |reactant plate/gas diffusion layer contact|
|           |resistance                              |
|t          |time                                    |
|UO2        |oxygen flowrate                         |
|UH2        |hydrogen flowrate                       |
```

Greek symbols
```
|?          |porosity                    |
|?          |resistivity                 |
|?          |torque                      |
```

Abbreviations
```
|DC         |direct current              |
|FEA        |finite element analysis     |
|GDL        |gas diffusin layer          |
|MEA        |membrane electrode assembly |
|PEMFC      |proton exchange membrane fuel cell|
|Pt         |platinum                    |
|RH         |relative humidity           |
|SA         |surface area                |
```

References

[1] M. F. Mathias, J. Roth, J. Fleming, W. Lehnert, Diffusion media materials and characterisation, in 'Handbook of Fuel Cells: Fundamentals, Technology and Applications, Volume 3, Chapter 42', W. Vielstich, A. Lamm and H. A. Gasteiger (Eds), John Wiley & Sons (2003) pp. 517 – 537.

[2] G. O. Mepsted, J. M. Moore, Performance and durability of bipolar plate materials, in 'Handbook of Fuel Cells: Fundamentals, Technology and Applications, Volume 3, Chapter 24', W. Vielstich, A. Lamm and H. A. Gasteiger (Eds), John Wiley & Sons (2003) pp. 286 – 293.

[3] D. A. Shores, G. A. Deluga, Basic materials corrosion issues, in 'Handbook of Fuel Cells: Fundamentals, Technology and Applications, Volume 3, Chapter 23', W. Vielstich, A. Lamm and H. A. Gasteiger (Eds), John Wiley & Sons (2003) pp. 273 – 284.

[4] V. Jalan and E. J. Taylor, Importance of Interatomic Spacing in Catalytic Reduction of Oxygen in Phosphoric Acid, J. Electrochemical Society 130 (1983) 2299 – 2302.

[5] S. J. Lee, C. D. Hsu, C. H. Huang Analyses of the fuel cell stack assembly pressure, J. Power Sources 145 (2005) 353 – 361.

[6] B. Zhang, X. Wang, Y. Song, Pressurized endplates for uniform pressure distributions in PEM fuel cells, in : Proceeding of the First International Conference on Fuel Cell Development and Deployment (2004).

[7] W. K. Lee, C. H. Ho, J. W. Van Zee, M. Murthy, The Effects of Compression and gas diffusion layers on the performance of a PEM fuel cell, J. Power Sources 84 (1999) 45 – 51.

[8] D. P. Wilkinson, O. Vanderleeden, Serpentine flow field design, in 'Handbook of Fuel Cells: Fundamentals, Technology and Applications, Volume 3, Chapter 27', W. Vielstich, A. Lamm and H. A. Gasteiger (Eds), John Wiley & Sons (2003) pp. 315 – 324.

[9] S. S. Kocha, Principles of MEA preparation, in 'Handbook of Fuel Cells: Fundamentals, Technology and Applications, Volume 3, Chapter 43', W. Vielstich, A. Lamm and H. A. Gasteiger (Eds), John Wiley & Sons (2003) pp. 550 – 565.

[10] S. Shimpalee, S. Greenway, D. Spuckler, J. W. Van Zee, Predicting water and current distributions in a commercial-size PEMFC, J. Power Sources 135 (2004) 79 – 87.

[11] J. Larminie, A. Dicks, Fuel Cell Systems Explained, John Wiley & Sons Ltd, ISBN 0 471 49026 1 (2003).

[12] A. McDougall, Fuel Cells, Macmillan (1976) pp 37 – 41.
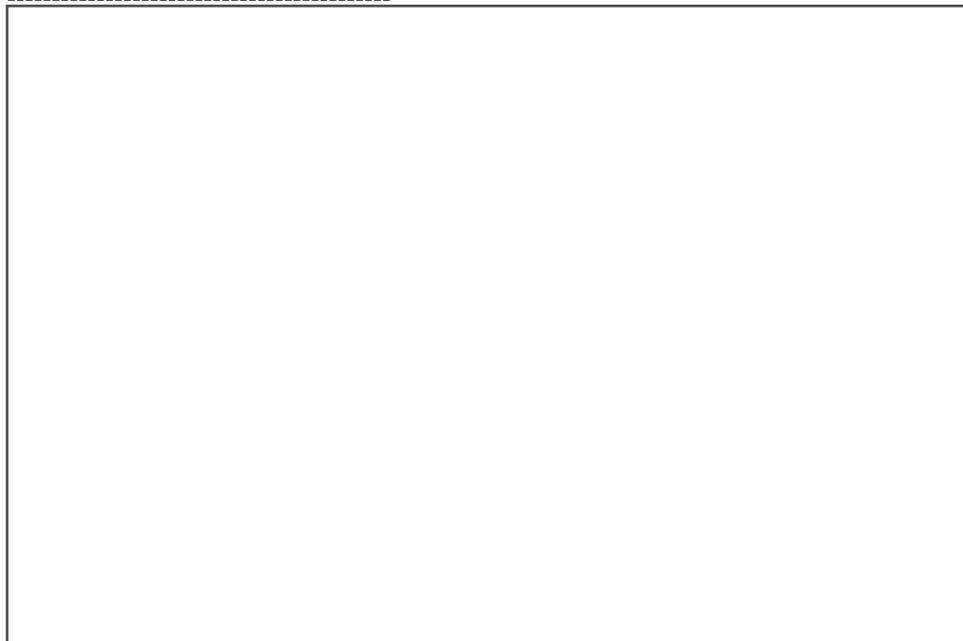
Current collector
RCC

Gas diffusion layer
RGDL

Reactant-flow plates
RRP

Catalyst RCA

Membrane
RM

Interfacial contact
resistance RCC/RP

RM

RCC

RRP/GDL

RCC/RP

RCA/M

RGDL/CA

RRP

RGDL

RCA

Air inlet

Fuel
Cell

PC
Data processing

Compression
unit

Humidity unit

Airflow controller

H2 flow controller

Load

Hydrogen inlet

Pressure sensors

Air outlet

Hydrogen outlet

Humidity and temperature sensors
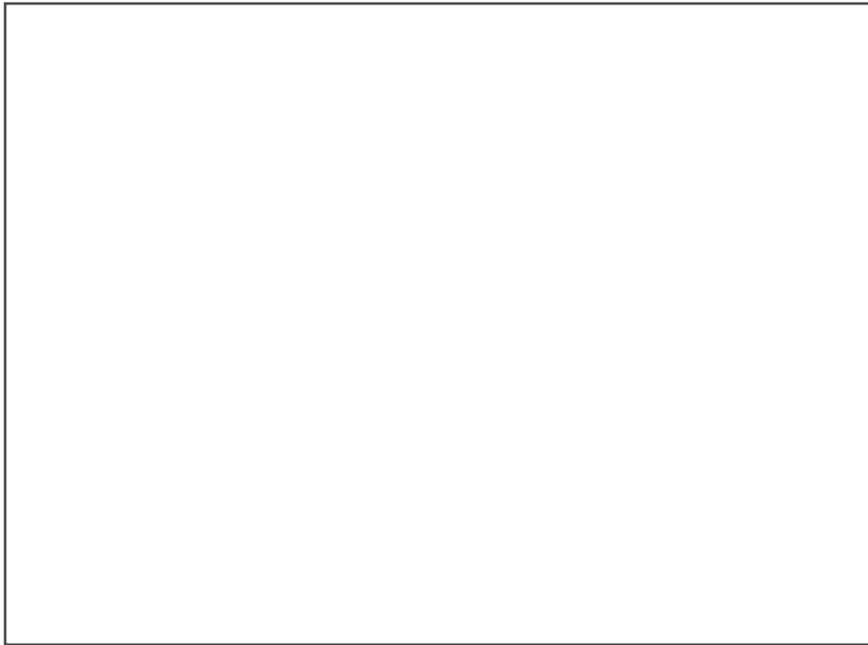
Top view

Fuel Cell

Applied Torque

Fuel cell inserted between the front plate and the pushing plate
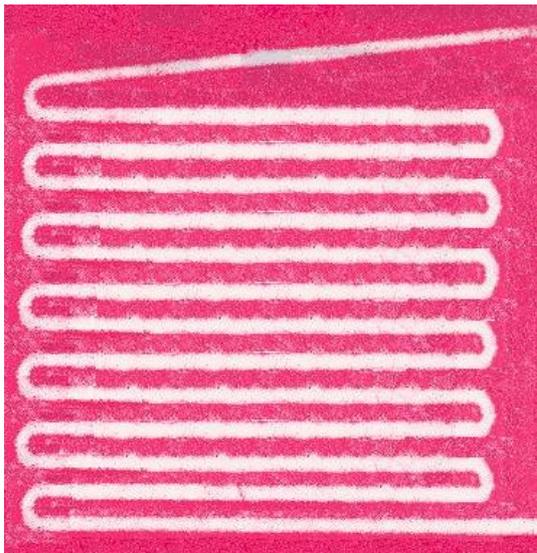
Compressive force
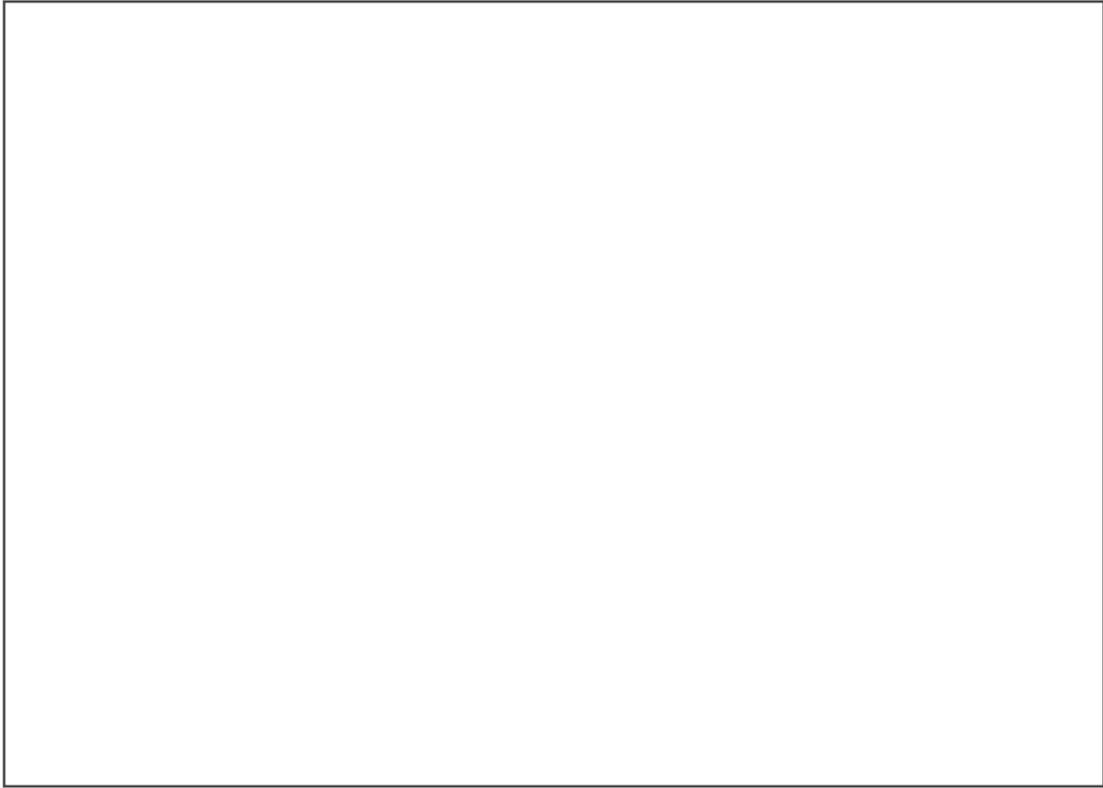
Back-screw

Pushing
plate

Side view

Front plate

Front plate

Pushing plate

Air Inlet

Air Outlet

Airflow channels

Plate strips

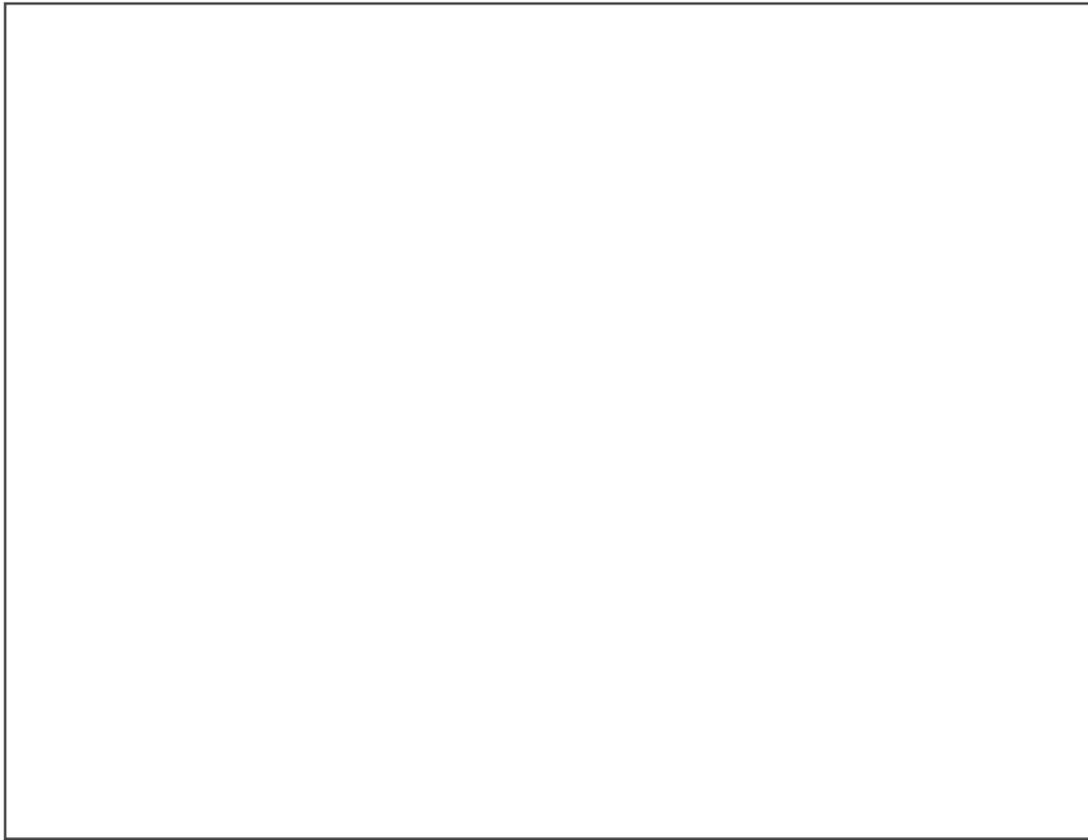| Toque (Nm)	8	10	12	14	16	18	20	22
Pressure (MNm-2)	0.8	1.4	2	2.6	3.3	3.9	4.4	5

(a)

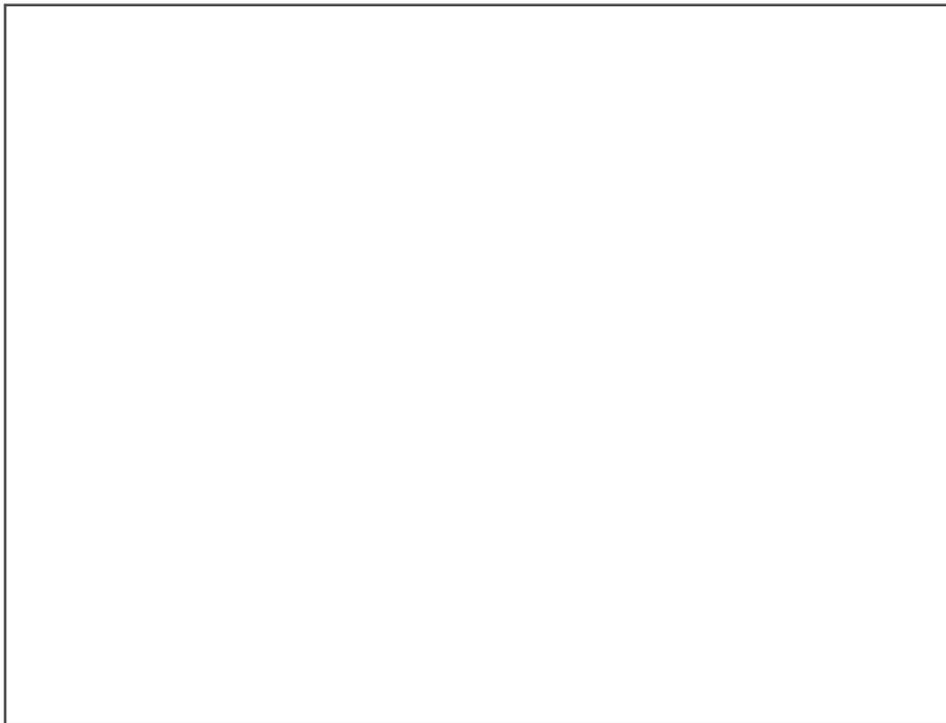(b)

(c)

(a) activation
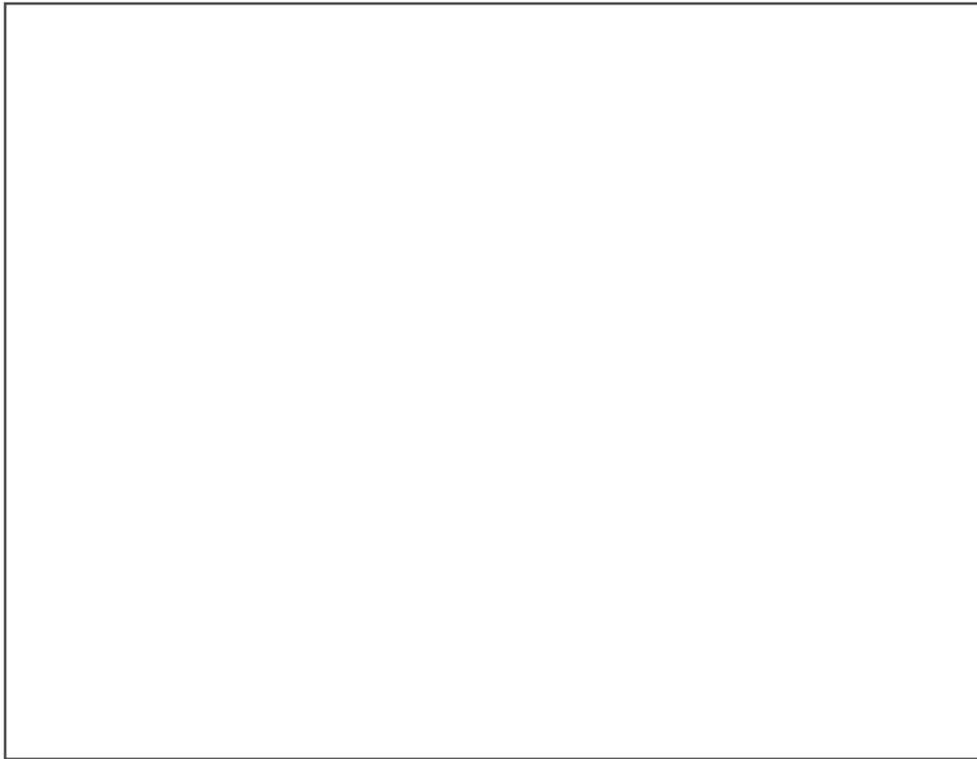(b) ohmic
(c) mass transport
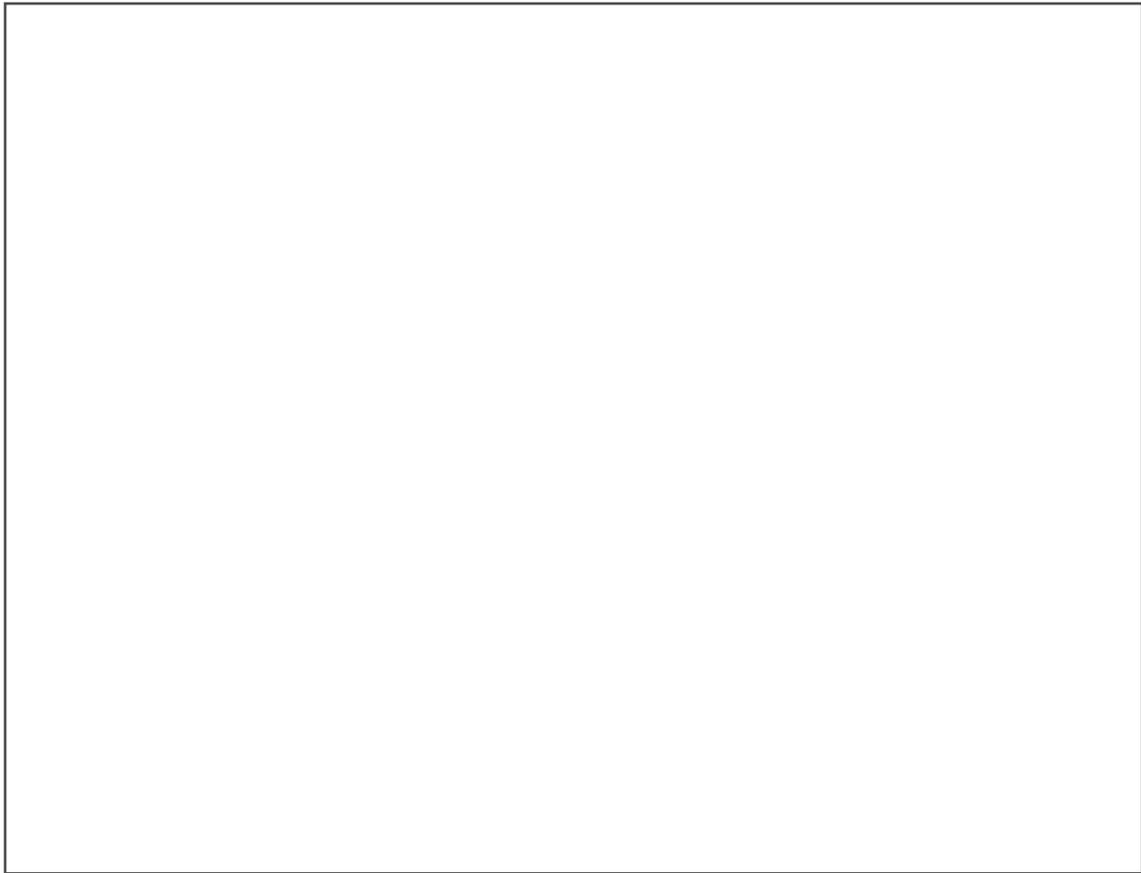
Faster
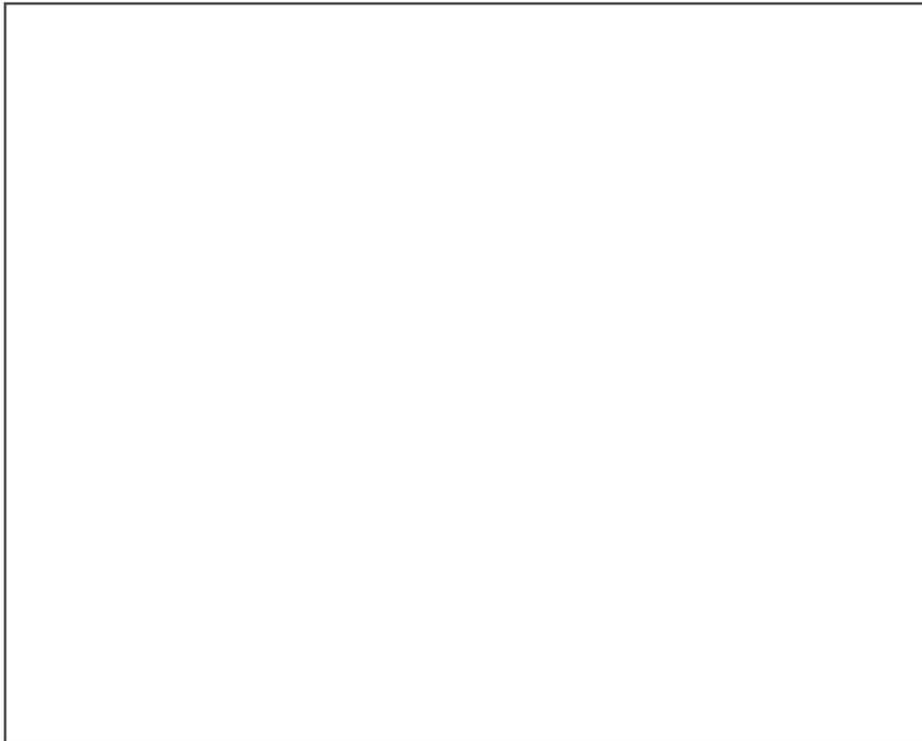reaction

Best-fit line intercepts the
current density axis at i0

Slower reaction

Slow reaction
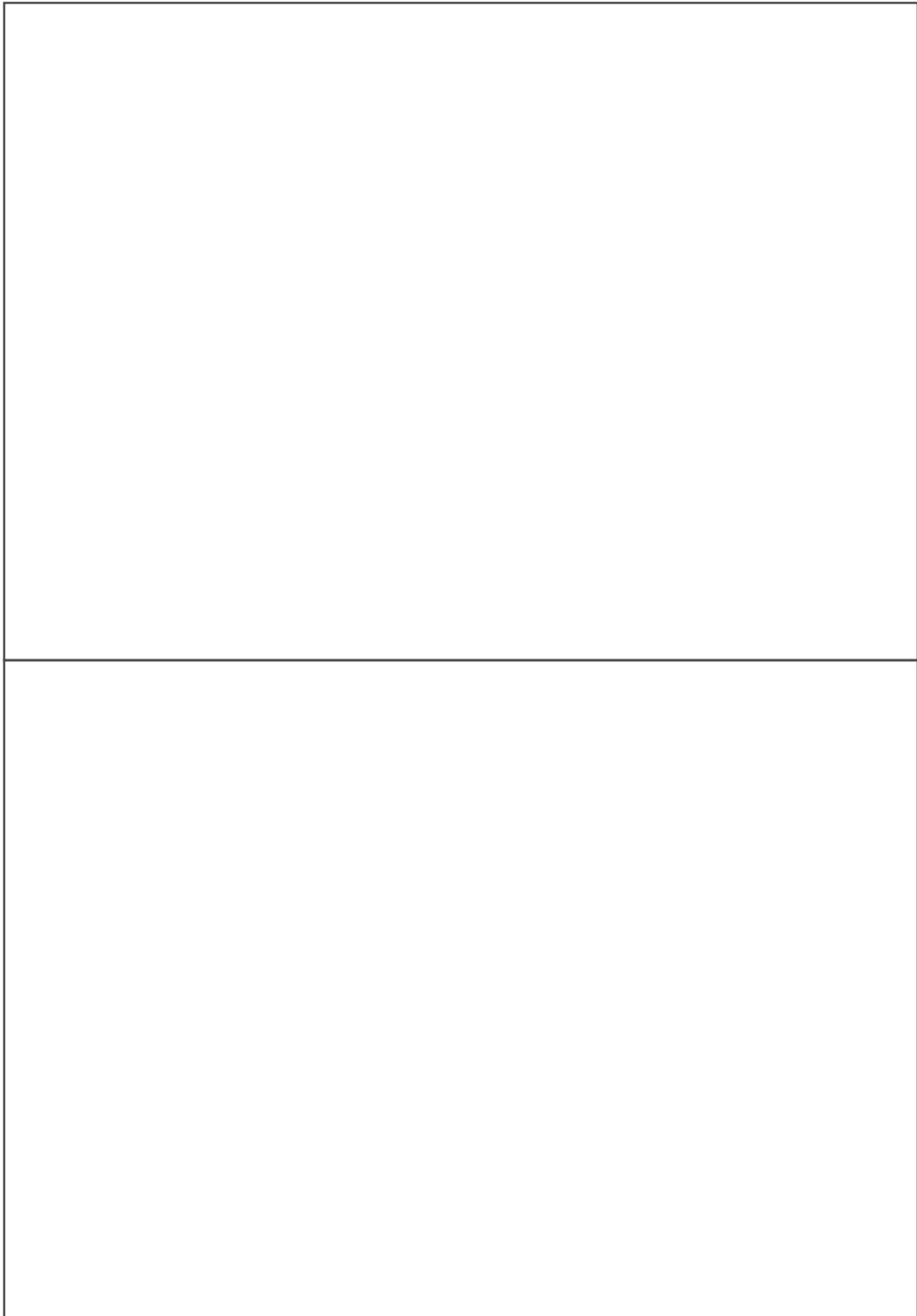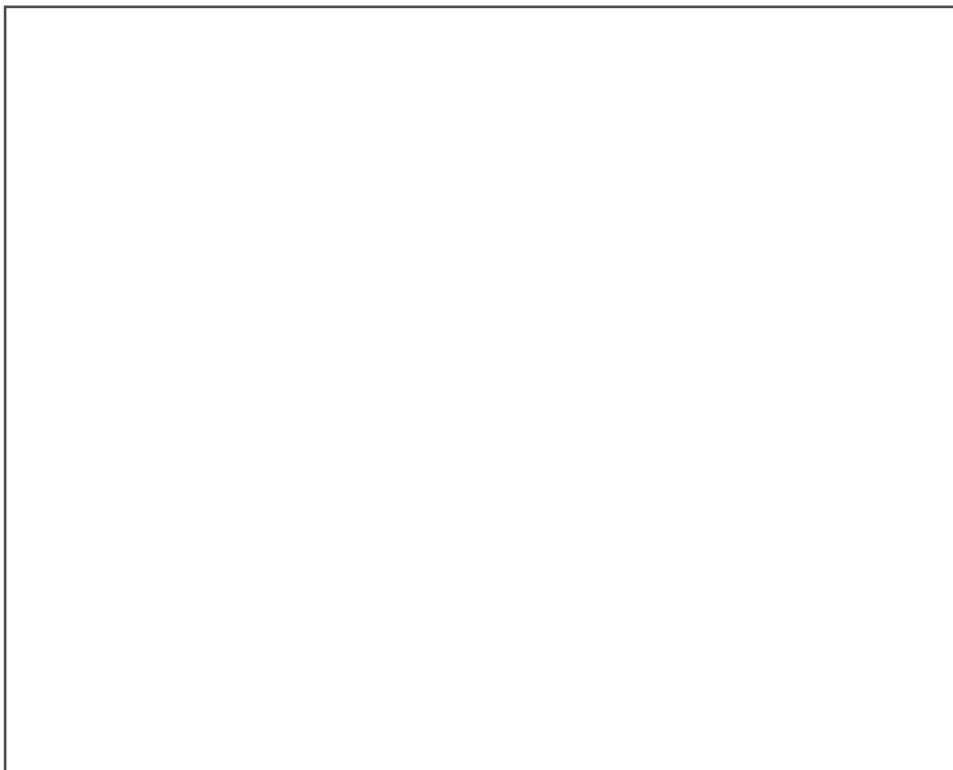
Region

Torque
(Nm)

Load
(Ohms)

?V
(mV)

?i
(mAcm-2)

10

0.33

0.01

Activation

Ohmic

Mass Transport

12
16
20

12
16
20

12
16
20

Total change
?i (mAcm-2)

Total change ?V (mV)

0.024
0.036
0.052

6.8
8.15
8

24
20.4
- 9.6

4
5
11

76
89
97

58
123
84

0.052

8

- 9.6

11

97

84